International Journal of Solids and Structures 53 (2015) 28–37

Contents lists available at ScienceDirect

International Journal of Solids and Structures

journal homepage: www.elsevier.com/locate/ijsolstr

The mode-coupling of a stiff film/compliant substrate system in the post-buckling range

Lijun Zhuo, Yin Zhang *

State Key Laboratory of Nonlinear Mechanics, Institute of Mechanics, Chinese Academy of Sciences, Beijing 100190, China

ARTICLE INFO

Article history:
Received 3 April 2014
Received in revised form 22 October 2014
Available online 1 November 2014

Keywords:
Period-doubling
Mode-coupling
Perturbation method
Substrate nonlinearities
Buckling/post-buckling

ABSTRACT

A compressed stiff film/compliant substrate system undergoes a morphology transition from wrinkling to period-doubling. The perturbation method is used to obtain the approximate analytical solution incorporating both the quadratic and cubic nonlinearities of the substrate, which have a significant effect on the post-buckling behavior of the system. Based on the perturbation method, the post-buckling equilibrium path of the system is presented with the multi-modal analysis, and two bifurcation points appear on the stable equilibrium path. The wrinkling instability occurs at the first bifurcation point, where the uncoupled path bifurcates from the fundamental unbuckled state. Under further compression, the period-doubling instability occurs at the second bifurcation point due to the coupling of different modes, which is referred to as the mode coupling. The two-mode analysis shows that the coupled equilibrium path is hyperbola-like and there exists a stable branch which bifurcates from the primary uncoupled path. When more modes are included, the model is more accurate to predict the critical strain of the period-doubling bifurcation and the evolution of the amplitudes.

1. Introduction

The compressed stiff film bonded to a compliant substrate can form wrinkles with a prescribed wavelength when the compression exceeds a critical value (Chen and Hutchinson, 2004; Huang, 2005; Huang et al., 2005). It has been observed widely in nature, ranging from human skins (Genzer and Groenewold, 2006) and tubular organs (Li et al., 2011) to fruits with hard pericarp and soft sarcocarp (Cerda and Mahadevan, 2003). Moreover, the buckling of the film/substrate system has been treated as a desirable means of generating controllable microscale surface pattern (Bowden et al., 1998, 1999). It also has some applications in the buckling-based metrology method (Stafford et al., 2004), microfluidic sieves (Kim and Crosby, 2011), microlens arrays (Chan and Crosby, 2006), tunable optical grating (Ma et al., 2013), and stretchable electronics (Khang et al., 2006; Jiang et al., 2008; Rogers et al., 2010).

However, recent investigations reveal that there exists a new buckling pattern beyond the sinusoidal wrinkling. Fig. 1 shows that the film/substrate system under a uniaxial compression firstly buckles into uniformly distributed sinusoidal wrinkles. Under further compression, the period-doubling instability appears at a relatively large deformation. Pocivavsek et al. (2008) experimentally investigated the wrinkle-to-fold transition of a polyester film resting on gel substrate and water, respectively. Particularly, the period-doubling instability was observed in the gel substrate case. The finite element simulations of an incompressible neo-Hookean bilayer (Cao and Hutchinson, 2012) and an elastic film with asymmetric bending stiffness on a hyperelastic substrate (Sun et al., 2011) showed the period-doubling morphology in the post-buckling regime. Although the buckling analysis based on linear substrate response is sufficient to predict the amplitude of the wrinkle in small strain range (Huang et al., 2005), many investigations have focused on the role of the substrate nonlinearity in the post-buckling instability of the system. Brau et al. (2011) revealed that the period-doubling instability is triggered by the quadratic nonlinearity of the substrate, which induces an up-down symmetry breaking: the tension and compression perpendicular to the surface of the substrate are no longer equivalent for the same given up/down displacement. Recently, Hutchinson (2013) studied the influence of the quadratic nonlinearity of a neo-Hookean substrate on the mode shape evolution of the hard film/soft substrate bilayer. In this study, the quadratic and cubic nonlinearities of the substrate will be both considered into the post-buckling analysis.

Previously, some researchers focused on the mode jumping of an axially compressed strut on a cubic nonlinear foundation. The primary buckling mode will lose stability at a secondary bifurcation point and experiences a sudden jump to a different buckling

* Corresponding author.
E-mail address: zhangyin@lnm.imech.ac.cn (Y. Zhang).

http://dx.doi.org/10.1016/j.ijsolstr.2014.10.028
0020-7683/

pattern of shorter wavelength (Everall and Hunt, 1999; Zhang and Murphy, 2005). Such jump is only possible when the coupled equilibrium path is elliptical, and only occurs from a lower mode to a higher mode (Hunt and Everall, 1999). For a strut on a full elastic foundation, the coupled path is unstable. In comparison, a partial elastic foundation can break the symmetry of the system and couple the modes to remain stable and thus avoid jumping (Zhang and Murphy, 2013). However, taking the quadratic nonlinearities of the substrate into account, an asymmetric and hyperbola-like coupled solution, which is similar to the case presented by Supple (1969), will bifurcate from the primary path of the uncoupled mode and couple the modes.

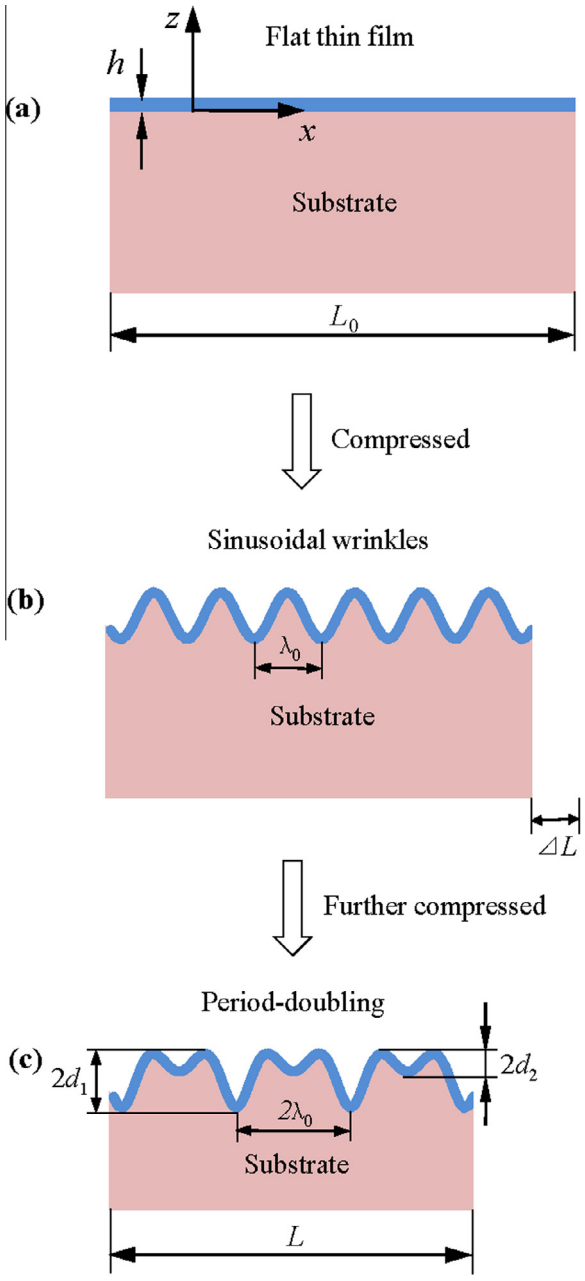

Fig. 1. A schematic of the film/substrate system and the coordinate system. (a) The undeformed state with initial length L_0 and film thickness h. (b) The sinusoidal wrinkles form when compressed by ΔL; λ_0 is the buckling wavelength. (c) The period-doubling configuration appears when compressed to a length of L; $2\lambda_0$ is the wavelength.

This paper explores the period-doubling instability of a compressed stiff film on a compliant substrate. Based on the perturbation method, some new analytical results on the nonlinear response of a half-space subject to periodic surface displacements are presented. The equilibrium equation which includes the quadratic and cubic nonlinearities is solved by the Ritz–Galerkin method and the post-buckling equilibrium paths are then obtained. The present model also predicts the critical strain of the period-doubling instability. The evolution of the mode amplitudes is compared with the experimental data obtained by Brau et al. (2011).

2. Model development

2.1. Governing equations of the thin film

Fig. 1 illustrates a hard film with the thickness h on a soft substrate. The bilayer system is initially flat before compression. It deforms only in the $x-z$ plane and is uniform along the y axis (perpendicular to the $x-z$ plane). In addition, the length in the y direction is much larger than the buckle wavelength, so the deformation of the system is plane-strain (Song et al., 2008). The top surface of the film is (assumed to be) traction free; the shear traction at the film/substrate interface is neglected because it has little effect on the solution of the film if the deflection is much smaller than the wavelength (Audoly and Boudaoud, 2008). Therefore, the film equation of equilibrium is the following ordinary differential equation:

$$D\frac{d^4w_f}{dx^4}+p\frac{d^2w_f}{dx^2}+q=0, \tag{1}$$

where $D=\bar{E}_f h^3/12$ is the film bending stiffness and w_f is the film deflection; $\bar{E}_f=E_f/(1-\nu_f^2)$ is the plane-strain modulus; E_f and ν_f are the film Young's modulus and Poisson's ratio, respectively; p is the film in-plane membrane force per unit width (positive for compression); q is the normal stress imposed on the film by the substrate, which will be derived later using the perturbation method.

2.2. The deformation of the substrate

The substrate is modeled as an isotropic elastic half-space (Volynskii et al., 2000; Song et al., 2008), with the Young's modulus of E_s and Poisson's ratio of ν_s. Although a linear substrate response is sufficient to predict the onset of wrinkling and the evolution of the wrinkle amplitude (e.g., Volynskii et al., 2000; Chen and Hutchinson, 2004), the geometric nonlinearity from the substrate is important for some post-buckling patterns and cannot be neglected for the case of large deformation. A general expression of the strain tensor ε_{ij} is written as follows (Landau and Lifshitz, 1959),

$$\varepsilon_{ij}=\frac{1}{2}\left(\frac{\partial u_i}{\partial x_j}+\frac{\partial u_j}{\partial x_i}+\frac{\partial u_k}{\partial x_i}\frac{\partial u_k}{\partial x_j}\right), \tag{2}$$

which is applicable to the slightly large deformation case. The equilibrium of force requires that

$$\frac{\partial \sigma_{ij}}{\partial x_j}=0. \tag{3}$$

Eq. (2) is essentially the Green strain according to Landau and Lifshitz (1959) and thus the stress in Eq. (3) is actually the second Piola–Kirchhoff stress. In this study, we consider a weakly nonlinear problem that there is no pre-stretch exerted on the substrate before compression of the film/substrate system. In addition, the period-doubling instability of the system only leads to small

stretching of the substrate (Brau et al., 2013). Hence we do not distinguish the reference state of deformation from the current state, and the deformation gradient is approximately uniform. As a result, the equilibrium equation corresponding to the second Piola–Kirchhoff stress is simplified to be the form as presented in Eq. (3). For a pre-stretched substrate, the current state of deformation is different from the reference state and the equilibrium equation should be written as $(F_{iK}\sigma_{JK})_J = 0$, where F_{iK} is the deformation gradient tensor (Song et al., 2008).

The stress tensor given by the Hookean elasticity is as follows:

$$\sigma_{ij} = 2G\varepsilon_{ij} + \lambda\varepsilon_{kk}\delta_{ij}, \tag{4}$$

where $i, j, k = 1$ or 3. The subscripts 1 and 3 represent the coordinates x and z in the undeformed state as shown in Fig. 1, respectively. The strain component ε_{22} is vanished for a plane strain deformation. $G = \frac{E_s}{2(1+\nu_s)}$ and $\lambda = \frac{E_s\nu_s}{(1+\nu_s)(1-2\nu_s)}$ are the Lamé constants, and δ_{ij} is the Kronecker delta function, namely,

$$\delta_{ij} = \begin{cases} 1, & i = j, \\ 0, & i \neq j. \end{cases} \tag{5}$$

It is noticed that Eq. (4) presents a linear stress–strain relation. According to Biot (1965), the linear stress–strain relation can capture the essential post-buckling features by retaining the nonlinear strain relation of Eq. (2). Furthermore, the experiment of Schneider et al. (2008) also physically verifies a linear stress–strain relationship of the polydimethylsiloxane (PDMS) up to a strain of 40%. In this study, PDMS is the substrate material and the material nonlinearity is thus not considered.

By substituting Eq. (2) and Eq. (4) into Eq. (3), the governing equation is given as follows

$$(1-2\nu_s)\nabla^2 u_i + \theta_{,i} + u_{k,ji}u_{k,j} + (1-2\nu_s)u_{k,i}u_{k,jj} = 0, \tag{6}$$

where $\nabla^2 = \frac{\partial^2}{\partial x_1^2} + \frac{\partial^2}{\partial x_3^2}$ is the Laplace operator, and $\theta = \frac{\partial u_1}{\partial x_1} + \frac{\partial u_3}{\partial x_3}$. For the half-space model, all the displacements are vanished far from the film/substrate interface (Groenewold, 2001), namely, $x_3 \to -\infty$. But the boundary conditions can be very different. For example, Song et al. (2008) imposed a vanishing shear traction at the interface; Huang (2005) and Mei et al. (2011) assumed that the shear and normal tractions at the interface are both nonzero. However, the film equation of equilibrium in Eq. (1) requires no shear traction at the interface. To determine the boundary conditions, the following assumptions Audoly and Boudaoud's (2008) are adopted:

(1) The film deflection is much smaller than the wavelength of the morphology;
(2) The ratio of the film Young's modulus to that of the substrate is large.

Based on the first assumption, the film in-plane displacements are much smaller than the out-of-plane displacement according to the scaling of the plate equations. From the substrate's perspective, the tangential displacement at the interface is thus assumed to be zero. According to the second assumption, the shear traction applied by the substrate at the interface is very small (if it is nonzero) and makes a negligible effect (Audoly and Boudaoud, 2008). Hence, we neglect the effect of the shear traction and assume the tangential displacement u_1 at the interface to be zero. Moreover, in order to study the response of the substrate when the coupled buckling mode appears, the transverse displacement u_3 should consist of two sinusoidal modes with different wave number. So the boundary conditions are imposed here as

$$\begin{cases} u_1(x_1, x_3 \to -\infty) = 0, \quad u_3(x_1, x_3 \to -\infty) = 0, \\ u_1(x_1, 0) = 0, \quad u_3(x_1, 0) = a\cos(kx_1) + b\cos(mkx_1), \end{cases} \tag{7}$$

where $k = 2\pi/\lambda$ is the wave number, and λ is the wavelength. a and b are the amplitudes, and m is a constant to indicate the difference in wave numbers between these two modes. $\cos(kx_1)$ is the primary mode indicating the uniform wrinkle. $\cos(mkx_1)$ is the secondary mode arising beyond the primary wrinkling. Particularly, the mode arising in the period-doubling instability can be written as $\cos(kx_1/2)$ by setting $m = 1/2$. In addition, the amplitude of the secondary mode should be much smaller than that of the primary mode near the onset of the period-doubling instability. For the amplitude is much smaller than the wavelength, we introduce a small parameter $\delta \sim a/\lambda$ (Song et al., 2008), and b is set to have a higher order than a, namely, $b/\lambda \sim \delta^2$.

The approximate analytical solution is obtained first by the perturbation method, and the stress imposed by the substrate (q) can then be derived/given in Eq. (1). The displacement components are expanded as the power series of δ, which gives the following

$$\begin{cases} u_1(x_1, x_3) = \lambda(U_1^{(0)} + \delta U_1^{(1)} + \delta^2 U_1^{(2)} + \cdots), \\ u_3(x_1, x_3) = \lambda(U_3^{(0)} + \delta U_3^{(1)} + \delta^2 U_3^{(2)} + \cdots), \end{cases} \tag{8}$$

where u_1 and u_3 are the in-plane and out-of-plane displacements, respectively; $U_1^{(i)}$ and $U_3^{(i)}$ are the ith order dimensionless functions to be determined. To satisfy the displacement boundary conditions in Eq. (7), where $u_3(x_1, 0)$ has no the zeroth order term, $U_3^{(0)}$ in Eq. (8) must vanish. On the other hand, all the displacement components are much smaller than the wavelength of λ, which implies that $U_1^{(0)}$ also need to vanish. The displacements in Eq. (8) are then substituted into Eq. (6) to get equations in the power series of δ, and all the terms with respect to different orders of δ should vanish. It yields a series of partial differential equations, which can be further reduced to a series of ordinary differential equations. As a result, solutions for the displacement components up to the order of δ^3 are derived (see Appendix A for details).

The strain components are expanded with respect to δ in the form

$$\begin{cases} \varepsilon_{11} = \delta\lambda U_{1,1}^{(1)} + \delta^2\lambda\left[U_{1,1}^{(2)} + \frac{\lambda}{2}\left(U_{1,1}^{(1)}\right)^2 + \frac{\lambda}{2}\left(U_{3,1}^{(1)}\right)^2\right] \\ \quad + \delta^3\lambda\left[U_{1,1}^{(3)} + \lambda U_{1,1}^{(1)}U_{1,1}^{(2)} + \lambda U_{3,1}^{(1)}U_{3,1}^{(2)}\right] + \cdots \\ \varepsilon_{33} = \delta\lambda U_{3,3}^{(1)} + \delta^2\lambda\left[U_{3,3}^{(2)} + \frac{\lambda}{2}\left(U_{1,3}^{(1)}\right)^2 + \frac{\lambda}{2}\left(U_{3,3}^{(1)}\right)^2\right] \\ \quad + \delta^3\lambda\left[U_{3,3}^{(3)} + \lambda U_{1,3}^{(1)}U_{1,3}^{(2)} + \lambda U_{3,3}^{(1)}U_{3,3}^{(2)}\right] + \cdots \end{cases} \tag{9}$$

where the expressions of $U_i^{(j)}$ are listed in Appendix A. In conjunction with Eq. (4), the normal stress component on the surface is as follows

$$\sigma_{33}(x_1, 0) = \frac{E_s(1-\nu_s)}{(1+\nu_s)(1-2\nu_s)}\left[\varepsilon_{33}(x_1, 0) + \frac{\nu_s}{1-\nu_s}\varepsilon_{11}(x_1, 0)\right], \tag{10}$$

which can be further expressed in the power series of δ by the substitution of the strain components in Eq. (9), namely,

$$\begin{aligned} \sigma_{33}(x_1, 0) = {} & \delta\lambda K_1 k[\cos(kx_1) + \delta m\cos(mkx_1)] \\ & + \delta^2 K_2 k^2\lambda^2\left[\cos^2(kx_1) - \frac{1}{2} + 2\delta m\cos(kx_1)\cos(mkx_1)\right] \\ & + \delta^3 K_3 k^3\lambda^3\cos^3(kx_1) + \delta^3 k^3\lambda^3 f_1\cos(kx_1) \\ & + \delta^3 k^2\lambda^2 f_2\cos[(1-m)kx_1] + \cdots, \end{aligned} \tag{11}$$

where $K_1 = \frac{2E_s(1-\nu_s)}{(3-4\nu_s)(1+\nu_s)}$, $K_2 = \frac{E_s(1-2\nu_s)(7-8\nu_s)}{2(3-4\nu_s)^2(1+\nu_s)}$, $K_3 = \frac{4E_s(1-\nu_s)^2}{3(3-4\nu_s)^3(1+\nu_s)}$. f_1 and f_2 are given as follows,

$$f_1 = \frac{192\nu_s^3 - 504\nu_s^2 + 454\nu_s - 141}{64(1-\nu_s^2)(3-4\nu_s)^3}E_s, \tag{12}$$

and

$$f_2 = \frac{mE_s[64v_s^3 - (8m+128)v_s^2 + (4m^2+6m+84)v_s - 4m^2 + m - 18]}{2(1+v_s)(3-4v_s)^3}. \tag{13}$$

An approximate form of Eq. (11) is given as follows

$$\sigma_{33}^*(x_1,0) = K_1k[a\cos(kx_1) + mb\cos(mkx_1)] + K_2k^2[a\cos(kx_1) + mb\cos(mkx_1)]^2 + K_3k^3[a\cos(kx_1)]^3, \tag{14}$$

where $a \sim \delta\lambda$ and $b \sim \delta^2\lambda$. When δ is relatively small, the difference between the perturbation solution of Eq. (11) and the approximate one of Eq. (14) is shown in Fig. 2(a) and (b). When δ approaches zero, both $\sigma_{33}(x_1, 0)$ and $\sigma_{33}^*(x_1, 0)$ become the degenerate solution of $\sigma_{33}^d(x_1, 0) = K_1ka\cos(kx_1)$, which is the normal stress of a linear substrate.

If the out-of-plane displacement on the surface $u_3(x_1, 0)$ is assumed as $a\cos(kx_1)$, namely, setting the amplitude b to be zero, the normal stress in Eq. (14) can be written as

$$\sigma_{33}^*(x_1,0) = K_1ku_3(x_1,0) + K_2k^2u_3^2(x_1,0) + K_3k^3u_3^3(x_1,0). \tag{15}$$

Here K_1k represents the linear stiffness of the substrate, which is consistent with the previous results (e.g., Biot, 1937; Groenewold, 2001; Chen and Hutchinson, 2004), for the case of incompressible substrate. K_2k^2 and K_3k^3 are the quadratic and cubic nonlinear stiffness, respectively. Fig. 3 illustrates that the substrate quadratic nonlinearity generates the stiffening effect for the outward displacements and the softening one for the inward displacements. Therefore, the substrate top surface tends to deform asymmetrically and favors the inward deformation. This trend is similar to the behavior of a pre-compressed neo-Hookean substrate subject to a periodic surface normal traction (Zang et al., 2012; Hutchinson, 2013). On the other hand, the cubic nonlinearity of the substrate generates the same stiffening effect for both the outward and the inward displacement which is symmetric.

2.3. Buckling and post-buckling analysis

The film is assumed to be perfectly bonded to the substrate, i.e., no delamination occurs (Mei et al., 2007). Furthermore, the deflection of the middle plane is assumed to be equal to that of the bottom surface for a thin film. So the film deflection is the same as the out-of-plane displacement on the surface of the substrate; and q exerted on the film in Eq. (1) is equal to the normal stress at the substrate surface, which gives the following two equations:

$$\begin{cases} w_f = u_3(x_1,0), \\ q = \sigma_{33}(x_1,0). \end{cases} \tag{16}$$

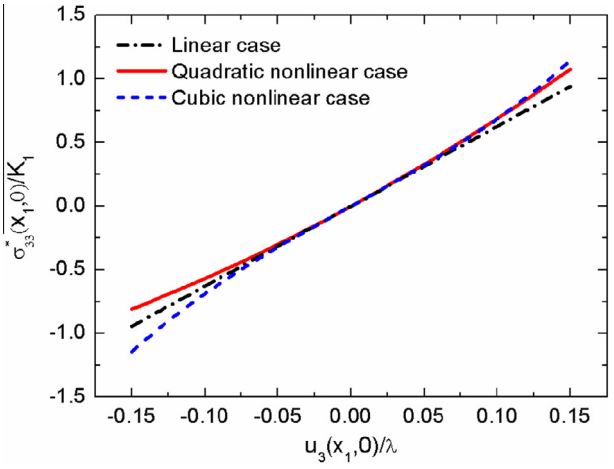

Fig. 3. The effects of substrate nonlinearities on the normal traction–displacement relationship as presented in Eq. (15).

For the primary buckling analysis in which the nonlinearity of the substrate is neglected, the film equation of equilibrium as given in Eq. (1) is now as the following:

$$D\frac{d^4w_f}{dx^4} + p\frac{d^2w_f}{dx^2} + K_1kw_f = 0, \tag{17}$$

where $p = \bar{E}_fh\varepsilon$ is the compressive membrane force and ε is the corresponding in-plane strain. The film deflection induced by the primary buckling is (assumed as) $w_f = a\cos kx$, where a is the amplitude and k is the wave number. By substituting this deflection into Eq. (17), the following equation is obtained (Biot, 1957; Chen and Hutchinson, 2004)

$$p = Dk^2 + K_1/k. \tag{18}$$

The smallest compressive membrane force determines the critical load of the primary buckling. So the bending of the film favors small wave number, whereas the deformation of the substrate favors large wave number. Consequently, the wrinkles select an intermediate one, which is the critical value, to minimize the membrane force. The critical wave number k_0 is determined by the vanishing of the differentiation of Eq. (18) with respect to k, namely

$$k_0 = \left(\frac{K_1}{2D}\right)^{\frac{1}{3}}. \tag{19}$$

The evolution of the amplitude can be derived by the inextensibility of the film (Cerda and Mahadevan, 2003; Pocivavsek et al., 2008; Brau et al., 2011), which is given as follows:

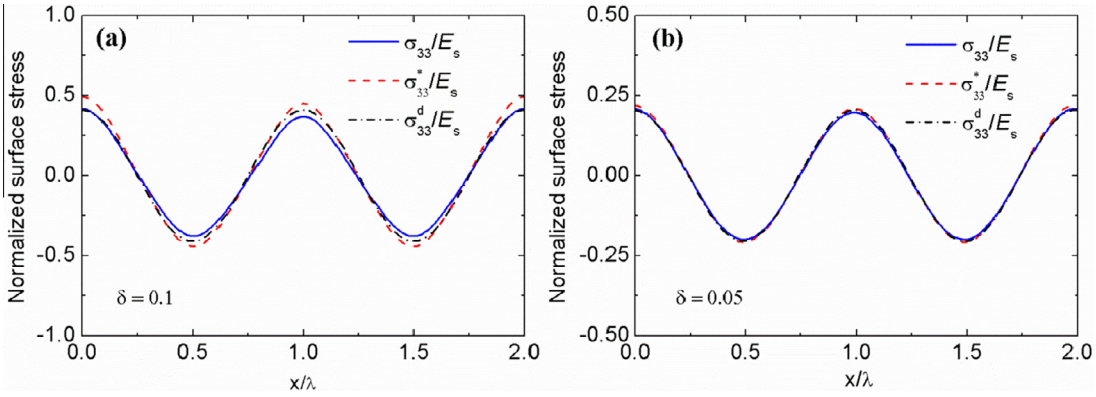

Fig. 2. Comparison of the perturbation solution of σ_{33}, its approximate form of σ_{33}^* and the degenerate solution of σ_{33}^d along the x-axis with Poisson's ratio $v_s = 0.48$ and $m = 1/2$ when (a) $\delta = 0.1$ and (b) $\delta = 0.05$.

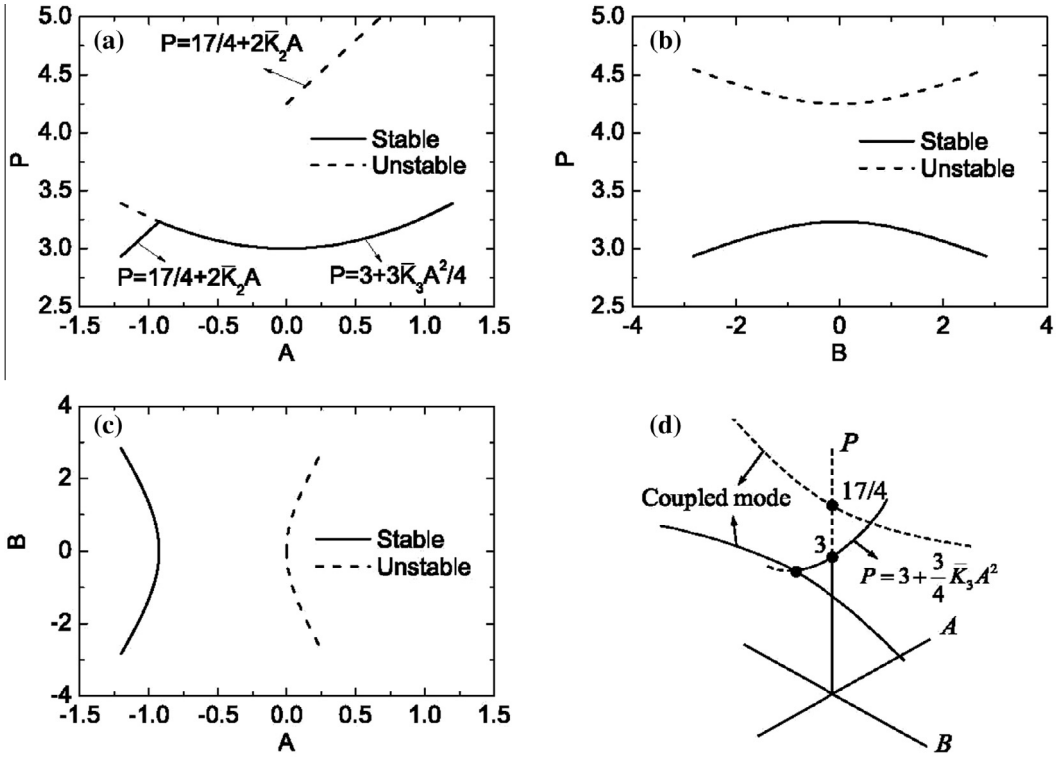

Fig. 4. The projections of the post-buckling equilibrium paths onto the (a) $P-A$, (b) $P-B$ and (c) $A-B$ planes, respectively. (d) The three-dimensional diagram of the paths. Stable paths are shown as solid lines and unstable paths as dashed lines.

$$\varepsilon_n = \frac{1}{\lambda_0}\int_0^{\lambda_0}\left(1-\sqrt{1-\left(\frac{dw_f}{dx}\right)^2}\right)dx, \tag{20}$$

where $\lambda_0 = 2\pi/k_0 = 2\pi(2D/K_1)^{1/3}$ is the critical wavelength, and $\varepsilon_n = \Delta L/L_0$ is the nominal overall compressive strain as illustrated in Fig. 1. By substituting the deflection of $w_f = a\cos kx$ into Eq. (20), the evolution of the amplitude as a function of the nominal overall strain is the following:

$$a = \frac{2}{k_0}\sqrt{\varepsilon_n} = \frac{\lambda_0}{\pi}\sqrt{\varepsilon_n}, \tag{21}$$

which has the same scale as the amplitude presented by Cerda and Mahadevan (2003) for the stretch-induced wrinkling. If the radical in Eq. (20) is expanded to the second order (Brau et al., 2011), the following equation is obtained

$$a = \frac{2}{k_0}\sqrt{\varepsilon_n}\left(1-\frac{3}{8}\varepsilon_n\right). \tag{22}$$

When the film/substrate system is further compressed beyond the onset of the primary buckling, a new configuration triggered by the period-doubling bifurcation as shown in Fig. 1(c) emerges (Pocivavsek et al., 2008; Brau et al., 2011; Cao and Hutchinson, 2012). This asymmetric morphology can be caused by the coupling of two or more sinusoidal modes with different wave number, because the coupled mode can bifurcate from the primary path of uncoupled mode under certain condition (Supple, 1967, 1969). Supple (1970) studied the changes of wave-form of a plate by discretizing the von Kármán plate equations based on the Ritz–Galerkin method, which is also used here to solve the governing equation of the film.

By setting the constant m in Eq. (7) to be 1/2, the deflection of the film is then written as $w_f = a\cos(k_0x) + b\cos(k_0x/2)$, where the wave number is assumed to be the critical value of the primary buckling and keeps a constant. As the system is further deformed, the effects of the substrate nonlinearities stand out. In conjunction with Eq. (16) and using the approximate stress σ_{33}^* of Eq. (14), the film governing equation is now obtained as follows:

$$D\frac{d^4w_f}{dx^4} + p\frac{d^2w_f}{dx^2} + K_1k_0\left[a\cos(k_0x) + \frac{b}{2}\cos\left(\frac{k_0x}{2}\right)\right] + K_2k_0^2\left[a\cos(k_0x) + \frac{b}{2}\cos\left(\frac{k_0x}{2}\right)\right]^2 + K_3k_0^3(a\cos(k_0x))^3 = 0. \tag{23}$$

The dimensionless form of Eq. (23) is

$$\frac{d^4W_f}{d\xi^4} + P\frac{d^2W_f}{d\xi^2} + 2\left[A\cos(\xi) + \frac{B}{2}\cos\left(\frac{\xi}{2}\right)\right] + \bar{K}_2\left[A\cos(\xi) + \frac{B}{2}\cos\left(\frac{\xi}{2}\right)\right]^2 + \bar{K}_3(A\cos(\xi))^3 = 0, \tag{24}$$

where $\xi = k_0x$ and other dimensionless parameters are listed as follows,

$$\begin{cases} W_f = w_fk_0, \quad A = ak_0, B = bk_0, \quad P = \frac{p}{Dk_0^2}, \\ \bar{K}_1 = \frac{K_1}{2Dk_0^3} = 1, \quad \bar{K}_2 = \frac{K_2}{Dk_0^3} = \frac{(1-2\nu_s)(7-8\nu_s)}{2(3-4\nu_s)(1-\nu_s)}, \quad \bar{K}_3 = \frac{K_3}{Dk_0^3} = \frac{4(1-\nu_s)}{3(3-4\nu_s)^2}. \end{cases} \tag{25}$$

Eq. (24) becomes the following two nonlinear algebraic equations by applying the Ritz–Galerkin method (see Appendix B for details)

$$\begin{cases} A(3-P) + \frac{1}{8}\bar{K}_2B^2 + \frac{3}{4}\bar{K}_3A^3 = 0, \\ B\left(\frac{17}{4} - P + 2\bar{K}_2A\right) = 0. \end{cases} \tag{26}$$

3. Results and discussion

Eq. (26) has the trivial solution of $A = B = 0$, which is referred to as the fundamental state of the film here. There are the following two nontrivial solutions:

$$\begin{cases} A \neq 0, & B = 0; \\ A \neq 0, & B \neq 0. \end{cases} \tag{27}$$

The first is referred to as the uncoupled mode and the second is the coupled mode. For the uncoupled mode, the first equation of Eq. (26) is simplified to

$$P = 3 + \frac{3}{4}\bar{K}_3 A^2. \tag{28}$$

Eq. (28) is the equilibrium path of the uncoupled mode triggered by the primary buckling, which is parabolic as shown in Fig. 4(a). Obviously, it bifurcates from the fundamental state at $P = 3$, and the corresponding (dimensional) membrane force is

$$p_c = 3Dk_0^2, \tag{29}$$

which is the same primary buckling load as given by Chen and Hutchinson (2004) for a incompressible substrate. If A and B are both nonzero, the following projections of the coupled mode onto the $P - A$ and $P - B$ planes are obtained by the second and the first equations of Eq. (26), respectively,

$$\begin{cases} P = \frac{17}{4} + 2\bar{K}_2 A, \\ (P-3)\left(P - \frac{17}{4}\right) - \frac{1}{4}(\bar{K}_2 B)^2 - \frac{3}{16}\frac{\bar{K}_3}{\bar{K}_2^2}\left(P - \frac{17}{4}\right)^3 = 0, \end{cases} \tag{30}$$

which are plotted in Fig. 4(a) and (b), respectively. Particularly, the projection on the $P - A$ plane is a straight line, which also intersects the uncoupled mode as shown in Fig. 4(a). The projection of the coupled mode onto the $A - B$ plane is further obtained by eliminating P in Eq. (26), which results in the following

$$6\bar{K}_3 A^3 - 16\bar{K}_2 A^2 - 10A + \bar{K}_2 B^2 = 0. \tag{31}$$

Eq. (31) is hyperbola-like as plotted in Fig. 4(c). The three-dimensional diagram of the equilibrium paths is presented in Fig. 4(d). However, without the effect of the quadratic nonlinearity, the coupled solution of Eq. (26) will degenerate into a straight line in the $P - A - B$ space, and there will be no period-doubling configuration. Furthermore, it is worth pointing out that only the branch with negative A is stable due to the smaller membrane force needed than that of the primary uncoupled mode. The other branch which bifurcates from the fundamental state is unstable. The configurations of the film on the stable and unstable coupled paths are shown in Fig. 5(a) and (b), respectively. Obviously, the period-doubling configuration appears on the stable path while the sinusoidal configuration with the doubled wavelength appears on the unstable path.

The amplitude of the primary mode at the mode coupling bifurcation point can be determined from Eq. (31) by setting $B = 0$. The corresponding critical nominal strain can thus be obtained by Eq. (21) as follows:

$$\varepsilon_{nc} = \left[\left(4\bar{K}_2 - \sqrt{16\bar{K}_2^2 + 15\bar{K}_3}\right)/(6\bar{K}_3)\right]^2. \tag{32}$$

It can be seen from Eqs. (30)–(32) that the coupled equilibrium paths as well as the critical strain depend on the substrate nonlinearities notably. Fig. 6 shows the projection of the stable coupled paths in the $A - B$ plane before and after eliminating the substrate cubic nonlinearity, respectively. It indicates that the cubic nonlinearity, which has the stiffening effect on the substrate, can decrease the amplitude of the primary mode when the mode coupling occurs, and thus a smaller nominal strain is needed.

As Eq. (25) shows that $\bar{K}_2$ and $\bar{K}_3$ only depend on the substrate Poisson's ratio v_s, Eq. (32) indicates that the critical strain for the period-doubling instability to occur is also dependent on v_s only. Fig. 7 plots the critical strain in Eq. (32) as a function of the Poisson's ratio between 0 and 0.5. The critical strain increases with increasing Poisson's ratio. If the substrate is nearly incompressible, $v_s = 0.48$, the critical strain ε_{nc} is about 50%, which is (much) higher as compared with the experimental data (Brau et al., 2011) and the numerical result (Cao and Hutchinson, 2012). More accuracy can be achieved by increasing the number of modes to approximate the film deflection as follows (Brau et al., 2011):

$$W_f = \sum_{i=1}^{n} C_i \cos\left(\frac{i\xi}{2}\right), \tag{33}$$

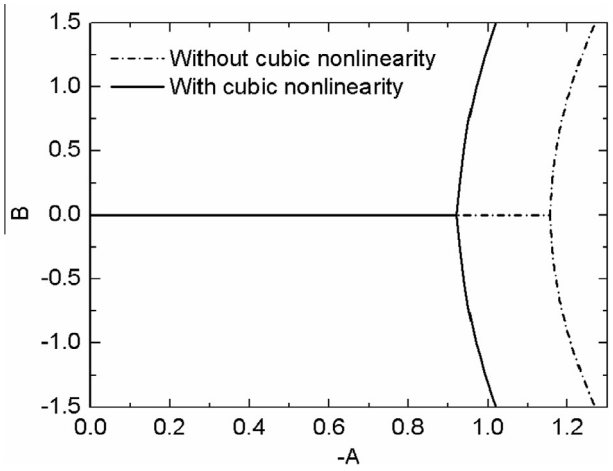

Fig. 6. The effect of the substrate cubic nonlinearity on the position of the bifurcation point at which mode coupling (period-doubling) begins. The solid and dashed lines indicate the stable coupled paths with and without the cubic nonlinearity, respectively.

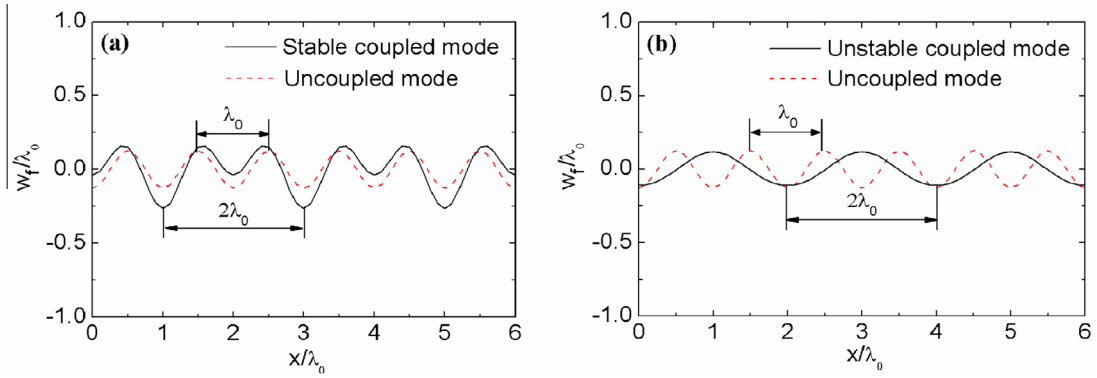

Fig. 5. The film configurations on the (a) stable coupled path at $(A, B) = (-0.95, 0.72)$ and (b) unstable coupled path at $(A, B) = (0.024, -0.72)$.

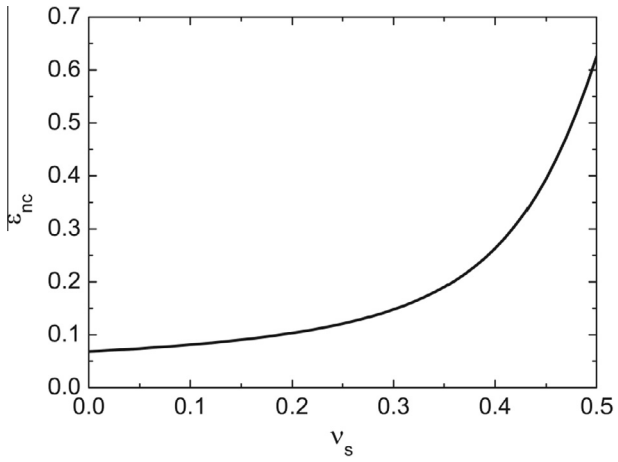

Fig. 7. Variation of the critical strain of period-doubling bifurcation shown in Eq. (32) as a function of the substrate Poisson's ratio ranging from 0 to 0.5.

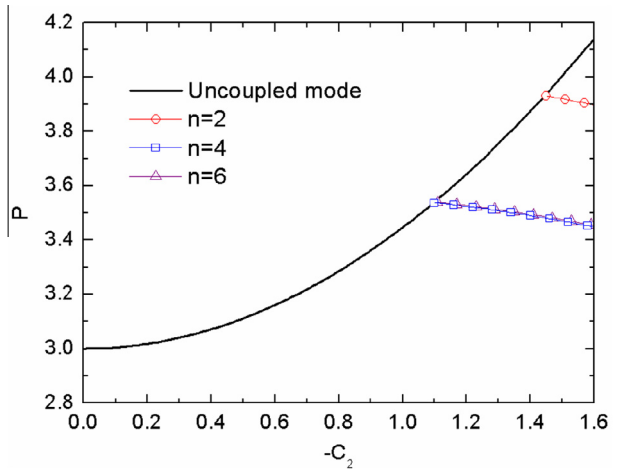

Fig. 8. Variations of the dimensionless membrane force P as a function of C_2 for the uncoupled mode and the stable coupled modes with n in Eq. (33) ranging from 2 to 6.

where $C_i = c_i k_0 (i = 1, 2 \ldots)$ and c_i is the amplitude of the ith mode; n is the mode number. In this form, c_2 indicates the amplitude of the primary buckling mode. By substituting Eq. (33) into Eq. (24), a series of the discretized equilibrium equations are derived by the Ritz–Galerkin method (See Appendix B for $n = 4$), and the solutions are obtained numerically by the Newton–Raphson method. The projections of the uncoupled path and the stable coupled path in the $P - C_2$ plane are demonstrated in Fig. 8 for mode number n varying from 2 to 6. The coupled paths hardly change when $n \geqslant 4$. Therefore, $n = 4$ is enough for the computational results to converge. Fig. 9(a) shows the evolution of the normalized amplitudes with respect to C_2. It indicates that there exists a simultaneous bifurcation in the values of C_1 and C_3 as C_2 increases, which is the reason for the occurrence of the period-doubling configuration. The film deflections before and after the bifurcation are shown in Fig. 9(b).

The value of the external nominal strain corresponding to each configuration can be derived based on the inextensibility of the film. By substituting the deflection in Eq. (33) into Eq. (20), the following relation between the nominal strain and the amplitudes is obtained when $n = 4$

$$\varepsilon_n = \frac{1}{16}\left(4C_1^2 + C_2^2 + 9C_3^2 + 16C_4^2\right). \tag{34}$$

The bifurcation point of $C_2 \approx -0.88$ as shown in Fig. 9(a) corresponds to the critical strain of about 20%. It is much closer to the experimental prediction and more accurate than the two-mode model, in which the critical strain is calculated about 33% for the same Poisson's ratio. Moreover, the amplitudes d_1 and d_2 characterizing the film morphology as shown in Fig. 1(c) are the functions of the normalized amplitudes C_i, which is given as follows

$$\begin{cases} \frac{d_1}{\lambda_0} = \frac{1}{4\pi}\left[W_f(\pi) - W_f(0)\right] = \frac{1}{4\pi}(-2C_2 - C_1 - C_3), \\ \frac{d_2}{\lambda_0} = \frac{1}{4\pi}\left[W_f(\pi) - W_f(2\pi)\right] = \frac{1}{4\pi}(-2C_2 + C_1 + C_3), \end{cases} \tag{35}$$

where C_1 and C_3 are both negative and much smaller than C_2. The evolutions of the film amplitudes as a function of the nominal strain ε_n based on the expansion in Eq. (22) are shown in Fig. 10 for the substrate Poisson's ratio ranging from 0.43 to 0.48. Comparing with the experiment carried by Brau et al. (2011) of a polydimethylsiloxane (PDMS) substrate cured with ultraviolet radiation–ozone, the theoretical evolutions of the amplitudes fit the experimental data well for ν_s varying from 0.43 to 0.44. But they deviate from the experiment when ν_s is 0.48, which is actually the Poisson's ratio closer to the material property of PDMS (Harrison et al., 2004; Song et al., 2008). This deviation may be caused by the assumption that the substrate is linear elastic (Hookean) as treated by Eq. (4) and the nonlinearity is from the large deformation only as indicated by Eq. (2). In reality, the constitutive relation of PDMS is nonlinear, which is treated as an incompressible neo-Hookean solid (Efimenko et al., 2005; Sun et al., 2011; Cao and Hutchinson, 2012; Hutchinson, 2013).

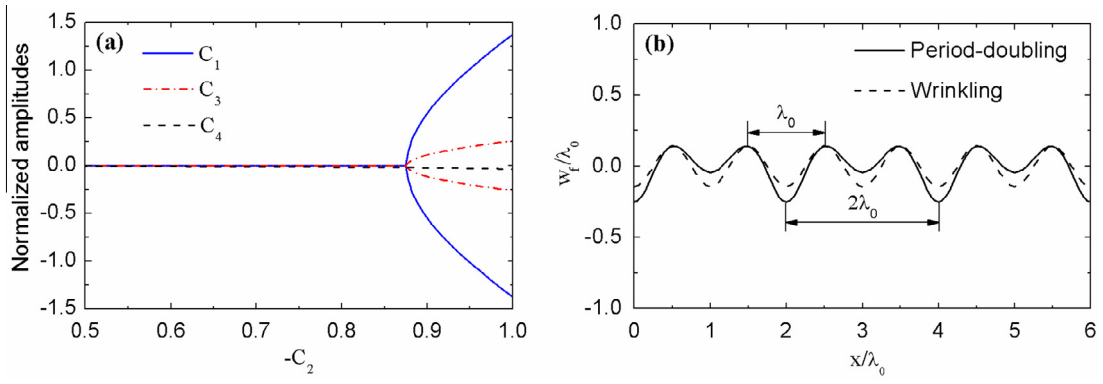

Fig. 9. (a) Variations of the normalized amplitudes as a function of C_2. (b) The film morphology before (dashed line) and after (solid line) the bifurcation. The substrate Poisson's ratio is 0.43.

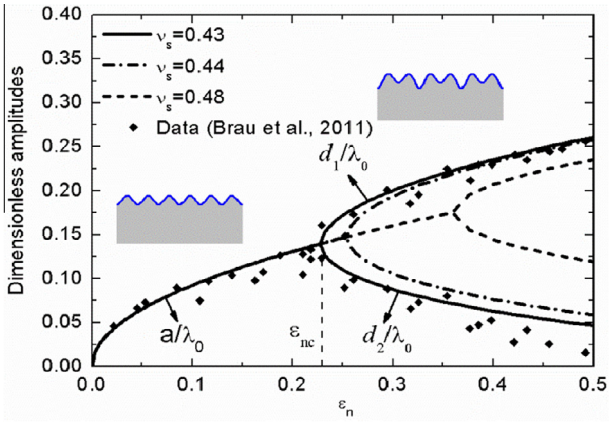

Fig. 10. Variation of the amplitudes d_1 and d_2 shown in Fig. 1(c) as a function of the nominal strain (ε_n) with different ν_s ranging from 0.43 to 0.48. The diamond symbols are the experimental data obtained by Brau et al. (2011).

4. Conclusions

The period-doubling configuration of a stiff thin film on a nonlinear substrate is induced by the coupling of several sinusoidal modes. If two modes participate in, the equilibrium path of the coupled mode is hyperbola-like. One of the branches bifurcates from the primary uncoupled mode and it is stable owing to the lower membrane force needed than that of the uncoupled mode. This bifurcation is triggered by the quadratic nonlinearity of the substrate, which has an asymmetric effect on the traction–displacement relationship of the substrate, and thus causes the symmetry-breaking of the surface configuration. Moreover, the cubic nonlinearity has a symmetric stiffening effect on both the tension and compression of the substrate, and thus the amplitude of the primary mode will be smaller when the period-doubling instability occurs as compared with that of the case without the cubic nonlinearity. As a result, the critical nominal strain is reduced. The evolution of the film morphology as a function of the nominal strain fits the experiment very well when four modes or more are used to approximate the film deflection and the substrate Poisson's ratio ν_s ranges from 0.43 to 0.44. The critical strain of the period-doubling bifurcation is only a function of the substrate Poisson's ratio and independent of the modulus ratio between the film and the substrate. Our future study is to incorporate both the constitutive and geometric nonlinearities.

Acknowledgment

The research has been supported by the National Natural Science Foundation of China (NSFC Nos. 11023001 and 11372321).

Appendix A. The response of the substrate under periodic displacement constraint

(i) *The expressions for* $U_1^{(1)}$ *and* $U_3^{(1)}$

All the terms with the order of δ should be vanished, leaving a series of partial differential equations related to $U_1^{(1)}$ and $U_3^{(1)}$,

$$\begin{cases} 2(1-\nu_s)U_{1,11}^{(1)} + (1-2\nu_s)U_{1,33}^{(1)} + U_{3,13}^{(1)} = 0, \\ (1-2\nu_s)U_{3,11}^{(1)} + 2(1-\nu_s)U_{3,33}^{(1)} + U_{1,13}^{(1)} = 0, \end{cases} \tag{A.1}$$

where ν_s is substrate Poisson's ratio. The boundary conditions can be obtained from Eq. (7) in the main text, namely,

$$\begin{cases} U_1^{(1)}(x_1, x_3 \to -\infty) = 0, \quad U_3^{(1)}(x_1, x_3 \to -\infty) = 0, \\ U_1^{(1)}(x_1, 0) = 0, \quad U_3^{(1)}(x_1, 0) = \cos(kx_1). \end{cases} \tag{A.2}$$

Assuming a decoupled form of those displacements, $U_1^{(1)} = F_1(kx_3)\sin(kx_1)$ and $U_3^{(1)} = F_3(kx_3)\cos(kx_1)$, Eq. (A.1) can be simplified to a series of ordinary differential equations

$$\begin{cases} F_1'''' - 2F_1'' + F_1 = 0, \\ (1-2\nu_s)F_1'' - 2(1-\nu_s)F_1 - F_3' = 0, \end{cases} \tag{A.3}$$

where the prime denotes differentiation with respect to x_3. The functions F_1 and F_3 satisfy the conditions: $F_1(-\infty) = F_3(-\infty) = 0$, $F_1(0) = 0$ and $F_3(0) = 1$. So Eq. (A.3) can be solved analytical and the expressions for $U_1^{(1)}$ and $U_3^{(1)}$ are

$$\begin{cases} U_1^{(1)} = \frac{1}{3-4\nu_s} kx_3 e^{kx_3}\sin(kx_1), \\ U_3^{(1)} = \frac{1}{3-4\nu_s}(3-4\nu_s-kx_3)e^{kx_3}\cos(kx_1). \end{cases} \tag{A.4}$$

(ii) *The expressions for* $U_1^{(2)}$ *and* $U_3^{(2)}$

To vanish the terms with the order of δ^2, $U_1^{(2)}$ and $U_3^{(2)}$ should satisfy the equations

$$\begin{cases} 2(1-\nu_s)U_{1,11}^{(2)} + (1-2\nu_s)U_{1,33}^{(2)} + U_{3,13}^{(2)} + \frac{2k^3\lambda(1-\nu_s)}{3-4\nu_s}e^{2kx_3}\sin(2kx_1) = 0, \\ (1-2\nu_s)U_{3,11}^{(2)} + 2(1-\nu_s)U_{3,33}^{(2)} + U_{1,13}^{(2)} - \frac{2k^3\lambda(1-\nu_s)}{3-4\nu_s}e^{2kx_3}\cos(2kx_1) \\ \quad + \frac{2k^3\lambda(2-5\nu_s+4\nu_s^2+2\nu_s kx_3+k^2x_3^2)}{(3-4\nu_s)^2}e^{2kx_3} = 0, \end{cases} \tag{A.5}$$

where the expressions for $U_1^{(1)}$ and $U_3^{(1)}$ has been substituted. The corresponding boundary conditions are listed as follows:

$$\begin{cases} U_1^{(2)}(x_1, x_3 \to -\infty) = 0, \quad U_3^{(2)}(x_1, x_3 \to -\infty) = 0, \\ U_1^{(2)}(x_1, 0) = 0, \quad U_3^{(2)}(x_1, 0) = \cos(mkx_1). \end{cases} \tag{A.6}$$

Here $U_1^{(2)}$ and $U_3^{(2)}$ are also set to be decoupled, namely

$$U_1^{(2)} = F_{11}(x_3)\sin(mkx_1) + F_{12}(x_3)\sin(2kx_1), \tag{A.7}$$

and

$$U_3^{(2)} = F_{31}(x_3)\cos(mkx_1) + F_{32}(x_3)\cos(2kx_1) + F_{33}(x_3). \tag{A.8}$$

With Eqs. (A.7) and (A.8), Eq. (A.5) can be simplified into a series of ordinary differential equations, and the solutions of the displacement components are

$$U_1^{(2)} = -\frac{(1-\nu_s)k\lambda}{(3-4\nu_s)^2}kx_3 e^{2kx_3}\sin(2kx_1) + \frac{1}{3-4\nu_s}mkx_3 e^{mkx_3}\sin(mkx_1), \tag{A.9}$$

and

$$\begin{aligned} U_3^{(2)} = {} & \frac{(1-\nu_s)k\lambda}{(3-4\nu_s)^2}kx_3 e^{2kx_3}\cos(2kx_1) \\ & + \frac{1}{3-4\nu_s}(3-4\nu_s-mkx_3)e^{mkx_3}\cos(mkx_1) \\ & + e^{2kx_3}\frac{k\lambda[(7-14\nu_s+8\nu_s^2)-4(1-\nu_s)kx_3+2k^2x_3^2]}{8(3-4\nu_s)^2(1-\nu_s)} \\ & - \frac{k\lambda[(7-14\nu_s+8\nu_s^2)]}{8(3-4\nu_s)^2(1-\nu_s)}. \end{aligned} \tag{A.10}$$

(iii) *The expressions for* $U_1^{(3)}$ *and* $U_3^{(3)}$

Similarly, leaving all the terms with the order of δ^3 to be zero, the governing equations for $U_1^{(3)}$ and $U_3^{(3)}$ are as follows:

$$\begin{aligned}
&2(1-v_s)U^{(3)}_{1,11}+(1-2v_s)U^{(3)}_{1,33}+U^{(3)}_{3,13}\\
&+\frac{e^{3kx_3}k^4\lambda^2\sin(kx_1)}{4(1-v_s)(3-4v_s)^3}\left[(34-92v_s+64v_s^2)k^2x_3^2\right.\\
&+(-6+8v_s)k^3x_3^3-(29-144v_s+236v_s^2-128v_s^3)kx_3\\
&\left.+56-300v_s+606v_s^2-552v_s^3+192v_s^4\right]\\
&-\frac{e^{3kx_3}k^4\lambda^2\sin(3kx_1)}{2(3-4v_s)^2}(7-15v_s+8v_s^2)\\
&+\frac{2k^3\lambda(1-v_s)m(1+m)e^{(1+m)kx_3}\sin[(1+m)kx_1]}{(3-4v_s)}\\
&-\frac{2k^3\lambda m(1-m)\left[5-15v_s+12v_s^2-(1-2v_s)(1+m)kx_3+mk^2x_3^2\right]}{(3-4v_s)^2}\\
&\times e^{(1+m)kx_3}\sin[(1-m)kx_1]=0,
\end{aligned}\tag{A.11}$$

and

$$\begin{aligned}
&(1-2v_s)U^{(3)}_{3,11}+2(1-v_s)U^{(3)}_{3,33}+U^{(3)}_{1,13}\\
&-\frac{e^{3kx_3}k^4\lambda^2\cos(kx_1)}{4(1-v_s)(3-4v_s)^3}\left[9-40v_s+102v_s^2-136v_s^3+64v_s^4\right.\\
&+(9+72v_s-212v_s^2+128v_s^3)kx_3+(64-164v_s+96v_s^2)k^2x_3^2\\
&\left.-(10-8v_s)k^3x_3^3\right]+\frac{e^{3kx_3}k^4\lambda^2\cos(3kx_1)}{2(3-4v_s)^2}(7-15v_s+8v_s^2)\\
&-\frac{2k^3\lambda(1-v_s)m(1+m)}{(3-4v_s)}e^{(1+m)kx_3}\cos[(1+m)kx_1]\\
&+\frac{2k^3\lambda me^{(1+m)kx_3}\cos[(1-m)kx_1]}{(3-4v_s)^2}\left[(2-5v_s+4v_s^2)(1+m)\right.\\
&\left.-(1-2v_s)(1+m^2)kx_3+2mkx_3+m(1+m)k^2x_3^2\right]=0,
\end{aligned}\tag{A.12}$$

and the corresponding boundary conditions are

$$\begin{cases}U_1^{(3)}(x_1,x_3\to-\infty)=0,\quad U_3^{(3)}(x_1,x_3\to-\infty)=0,\\ U_1^{(3)}(x_1,0)=0,\quad U_3^{(3)}(x_1,0)=0.\end{cases}\tag{A.13}$$

Here $U_1^{(3)}$ and $U_3^{(3)}$ are also assumed to have a decoupled form, namely,

$$\begin{cases}U_1^{(3)}=G_{11}\sin(kx_1)+G_{12}\sin(3kx_1)+G_{13}\sin[(1+m)kx_1]\\ +G_{14}\sin[(1-m)kx_1],\\ U_3^{(3)}=G_{31}\cos(kx_1)+G_{32}\cos(3kx_1)+G_{33}\cos[(1+m)kx_1]\\ +G_{34}\cos[(1-m)kx_1],\end{cases}\tag{A.14}$$

where $G_{ij}(i=1\text{ or }3, j=1\text{ to }4)$ is the functions of x_3 to be determined. By substituting Eq. (A.14) into Eq. (A.11) and Eq. (A.12), G_{ij} is solved analytically and presented as follows:

$$\begin{aligned}
G_{11}=&\frac{k^2\lambda^2}{(1-v_s)^2(3-4v_s)^3}\left\{e^{kx_3}\left[\frac{253-760v_s+768v_s^2-256v_s^3}{512}kx_3\right.\right.\\
&+\frac{1621}{512}-\frac{757v_s}{64}+\frac{277v_s^2}{16}-\frac{93v_s^3}{8}+3v_s^4\Big]\\
&-e^{3kx_3}\left[\frac{-9+8v_s}{64}k^3x_3^3+\left(\frac{131}{128}-2v_s+v_s^2\right)k^2x_3^2\right.\\
&+\left(-\frac{1125}{512}+\frac{195v_s}{32}-\frac{95v_s^2}{16}+2v_s^3\right)kx_3\\
&\left.\left.+\frac{1621}{512}-\frac{757v_s}{64}+\frac{277v_s^2}{16}-\frac{93v_s^3}{8}+3v_s^4\right]\right\},
\end{aligned}\tag{A.15}$$

$$G_{12}=\frac{k^2\lambda^2(1-v_s)(7-8v_s)}{6(3-4v_s)^3}kx_3e^{3kx_3},\tag{A.16}$$

$$G_{13}=\frac{-2k\lambda m(1-v_s)}{(3-4v_s)^2}kx_3e^{(1+m)kx_3},\tag{A.17}$$

$$\begin{aligned}
G_{14}=&\frac{2k\lambda m^2(1-m)}{(1-v_s)(3-4v_s)^2}\left\{e^{(1+m)kx_3}\left[\frac{k^2x_3^2}{8m}+\frac{(4v_s-5)(1+m)}{16m^2}kx_3\right.\right.\\
&\left.+\frac{1+m^2(1-v_s)-v_s}{4m^3}+\frac{8-19v_s+12v_s^2}{8m^2}\right]\\
&-e^{(1-m)kx_3}\left[\frac{1+m^2(1-v_s)-v_s}{4m^3}+\frac{8-19v_s+12v_s^2}{8m^2}\right.\\
&\left.\left.+\frac{(3-4v_s)^2-8m^2(1-v_s)+m(-15+44v_s-32v_s^2)}{16m^2(3-4v_s)}kx_3\right]\right\},
\end{aligned}\tag{A.18}$$

$$\begin{aligned}
G_{31}=&\frac{k^2\lambda^2}{(1-v_s)^2(3-4v_s)^3}\left\{e^{3kx_3}\left[\frac{-11+8v_s}{64}k^3x_3^3+\left(\frac{187}{128}-\frac{47}{16}v_s+\frac{3}{2}v_s^2\right)k^2x_3^2\right.\right.\\
&\left.+\left(-\frac{1063}{512}+\frac{93v_s}{16}-\frac{93v_s^2}{16}+2v_s^3\right)kx_3+\frac{431}{256}-\frac{691v_s}{128}+\frac{55v_s^2}{8}-\frac{33v_s^3}{8}+v_s^4\right]\\
&-e^{kx_3}\left[\frac{253-760v_s+768v_s^2-256v_s^3}{512}kx_3\right.\\
&\left.\left.+\frac{431}{256}-\frac{563v_s}{128}+\frac{55v_s^2}{8}-\frac{33v_s^3}{8}\right]\right\},
\end{aligned}\tag{A.19}$$

$$G_{32}=-\frac{k^2\lambda^2(1-v_s)(7-8v_s)}{6(3-4v_s)^3}kx_3e^{3kx_3},\tag{A.20}$$

$$G_{33}(X_3)=\frac{2mk\lambda(1-v_s)}{(3-4v_s)^2}kx_3e^{(1+m)kx_3},\tag{A.21}$$

$$\begin{aligned}
G_{34}=&\frac{k\lambda}{8m(1-v_s)(3-4v_s)^2}\left\{-e^{(1+m)kx_3}\left[2(m^2+m^3)k^2x_3^2\right.\right.\\
&+(4v_s-5)(m+m^3)kx_3+2m^2kx_3+4(1-v_s)(1+m^3)\\
&\left.+(m+m^2)(1-2v_s)(3-4v_s)\right]\\
&+e^{(1-m)kx_3}\left[m(3-4v_s)kx_3-m^2(8-12v_s)kx_3\right.\\
&+\frac{8m^4(1-v_s)+m^3(7-36v_s+32v_s^2)}{(3-4v_s)}kx_3\\
&\left.\left.+4(1+m^3)(1-v_s)+(m+m^2)(3-10v_s+8v_s^2)\right]\right\}.
\end{aligned}\tag{A.22}$$

Appendix B. The discretized equilibrium equations of the film

For the case of $n=2$, $W_f=A\cos(\xi)+B\cos(\xi/2)$, Eq. (24) can be discretized into two nonlinear algebraic equations by Ritz–Galerkin method, namely,

$$\begin{cases}\int_0^{2\pi/k_0}\cos(\xi)\left(\frac{d^4W_f}{d\xi^4}+P\frac{d^2W_f}{d\xi^2}+\bar\sigma^*_{33}\right)dx=0,\\ \int_0^{2\pi/k_0}\cos(\frac{\xi}{2})\left(\frac{d^4W_f}{d\xi^4}+P\frac{d^2W_f}{d\xi^2}+\bar\sigma^*_{33}\right)dx=0,\end{cases}\tag{B.1}$$

where

$$\begin{aligned}
\bar\sigma^*_{33}=&2\left[A\cos(\xi)+\frac{B}{2}\cos\left(\frac{\xi}{2}\right)\right]\\
&+\bar K_2\left[A\cos(\xi)+\frac{B}{2}\cos\left(\frac{\xi}{2}\right)\right]^2+\bar K_3(A\cos(\xi))^3.
\end{aligned}\tag{B.2}$$

Eq. (B.1) is further simplified into Eq. (26) in the main text. For the case of $n = 4$, the film dimensionless deflection is $W_f = C_1 \cos(\xi/2) + C_2 \cos(\xi) + C_3 \cos(3\xi/2) + C_4 \cos(2\xi)$, and four nonlinear algebraic equations for the normalized amplitudes and the dimensionless membrane force are derived as follows:

$$\begin{cases} \bar{K}_2 C_1 (C_1 + 6C_3) + 6\bar{K}_3 C_2^3 + 8C_2(3 + 2\bar{K}_2 C_4 - P) = 0, \\ 24\bar{K}_2 C_3 (C_2 + 2C_4) + C_1(17 + 8\bar{K}_2 C_2 - 4P) = 0, \\ 8\bar{K}_2 C_1 (C_2 + 2C_4) + C_3(129 - 36P) = 0, \\ (2C_2^2 + 3C_1 C_3)\bar{K}_2 + 16C_4(5 - P) = 0. \end{cases} \tag{B.3}$$

These equations can be solved numerical by the Newton–Raphson method, as long as one of the unknown parameters is prescribed at first. Here all the normalized amplitudes in Eq. (B.3) can be expressed as a function of P, giving the evolution of the film shape as the membrane force varies.

References

Audoly, B., Boudaoud, A., 2008. Buckling of a stiff film bound to a compliant substrate—Part I: formulation, linear stability of cylindrical patterns, secondary bifurcations. J. Mech. Phys. Solids 56 (7), 2401–2421.

Biot, M.A., 1937. Bending of an infinite beam on an elastic foundation. J. Appl. Mech. 4 (1937), A1–A7.

Biot, M.A., 1957. Folding instability of a layered viscoelastic medium under compression. Proc. R. Soc. A 242 (1231), 444–454.

Biot, M.A., 1965. Mechanics of Incremental Deformations. John Wiley & Sons Inc, New York.

Bowden, N., Brittain, S., Evans, A.G., Hutchinson, J.W., Whitesides, G.M., 1998. Spontaneous formation of ordered structures in thin films of metals supported on an elastomeric polymer. Nature 393 (6681), 146–149.

Bowden, N., Huck, W.T.S., Paul, K.E., Whitesides, G.M., 1999. The controlled formation of ordered, sinusoidal structures by plasma oxidation of an elastomeric polymer. Appl. Phys. Lett. 75 (17), 2557–2559.

Brau, F., Vandeparre, H., Sabbah, A., Poulard, C., Boudaoud, A., Damman, P., 2011. Multiple-length-scale elastic instability mimics parametric resonance of nonlinear oscillators. Nat. Phys. 7 (1), 56–60.

Brau, F., Damman, P., Diamant, H., Witten, T.A., 2013. Wrinkle to fold transition: influence of the substrate response. Soft Matter 9 (34), 8177–8186.

Cao, Y.P., Hutchinson, J.W., 2012. Wrinkling phenomena in neo-Hookean film/substrate bilayers. J. Appl. Mech. 79 (3), 031019.

Cerda, E., Mahadevan, L., 2003. Geometry and physics of wrinkling. Phys. Rev. Lett. 90 (7), 074302.

Chan, E.P., Crosby, A.J., 2006. Fabricating microlens arrays by surface wrinkling. Adv. Mater. 18 (24), 3238–3242.

Chen, X., Hutchinson, J.W., 2004. Herringbone buckling patterns of compressed thin films on compliant substrates. J. Appl. Mech. 71 (5), 597–603.

Efimenko, K., Rackaitis, M., Manias, E., Vaziri, A., Mahadevan, L., Genzer, J., 2005. Nested self-similar wrinkling patterns in skins. Nat. Mater. 4 (4), 293–297.

Everall, P.R., Hunt, G.W., 1999. Quasi-periodic buckling of an elastic structure under the influence of changing boundary conditions. Proc. R. Soc. A 455 (1988), 3041–3051.

Genzer, J., Groenewold, J., 2006. Soft matter with hard skin: from skin wrinkles to templating and material characterization. Soft Matter. 2 (4), 310–323.

Groenewold, J., 2001. Wrinkling of plates coupled with soft elastic media. Physica A 298 (1–2), 32–45.

Harrison, C., Stafford, C.M., Zhang, W., Karim, A., 2004. Sinusoidal phase grating created by a tunably buckled surface. Appl. Phys. Lett. 85 (18), 4016.

Huang, R., 2005. Kinetic wrinkling of an elastic film on a viscoelastic substrate. J. Mech. Phys. Solids 53 (1), 63–89.

Huang, Z.Y., Hong, W., Suo, Z., 2005. Nonlinear analyses of wrinkles in a film bonded to a compliant substrate. J. Mech. Phys. Solids 53 (9), 2101–2118.

Hunt, G.W., Everall, P.R., 1999. Arnold tongues and mode-jumping in the supercritical post-buckling of an archetypal elastic structure. Proc. R. Soc. A 455 (1981), 125–140.

Hutchinson, J.W., 2013. The role of nonlinear substrate elasticity in the wrinkling of thin films. Phil. Trans. R. Soc. A 371 (1993), 20120422.

Jiang, H., Sun, Y., Rogers, J.A., Huang, Y., 2008. Post-buckling analysis for the precisely controlled buckling of thin film encapsulated by elastomeric substrates. Int. J. Solids Struct. 45 (7–8), 2014–2023.

Khang, D.-Y., Jiang, H., Huang, Y., Rogers, J.A., 2006. A stretchable form of single-crystal silicon for high-performance electronics on rubber substrates. Science 311 (5758), 208–212.

Kim, H.S., Crosby, A.J., 2011. Solvent-responsive surface via wrinkling instability. Adv. Mater. 23 (36), 4188–4192.

Landau, L.D., Lifshitz, E.M., 1959. Theory of elasticity. Pergamon, New York.

Li, B., Cao, Y.P., Feng, X.Q., Gao, H.J., 2011. Surface wrinkling of mucosa induced by volumetric growth: theory, simulation and experiment. J. Mech. Phys. Solids 59 (4), 758–774.

Ma, T., Liang, H., Chen, G., Poon, B., Jiang, H., Yu, H., 2013. Micro-strain sensing using wrinkled stiff thin films on soft substrates as tunable optical grating. Opt. Express 21 (10), 11994–12001.

Mei, H.X., Huang, R., Chung, J.Y., Stafford, C.M., Yu, H.H., 2007. Buckling modes of elastic thin films on elastic substrates. Appl. Phys. Lett. 90 (15), 151902.

Mei, H.X., Landis, C.M., Huang, R., 2011. Concomitant wrinkling and buckle-delamination of elastic thin films on compliant substrates. Mech. Mater. 43 (11), 627–642.

Pocivavsek, L., Dellsy, R., Kern, A., Johnson, S., Lin, B., Lee, K.Y.C., Cerda, E., 2008. Stress and fold localization in thin elastic membranes. Science 320 (5878), 912–916.

Rogers, J.A., Someya, T., Huang, Y., 2010. Materials and mechanics for stretchable electronics. Science 327 (5973), 1603–1607.

Schneider, F., Fellner, T., Wilde, J., Wallrabe, U., 2008. Mechanical properties of silicones for MEMS. J. Micromech. Microeng. 18 (6), 065008.

Song, J., Jiang, H., Liu, Z.J., Khang, D.Y., Huang, Y., Rogers, J.A., Lu, C., Koh, C.G., 2008. Buckling of a stiff thin film on a compliant substrate in large deformation. Int. J. Solids Struct. 45 (10), 3107–3121.

Stafford, C.M., Harrison, C., Beers, K.L., Karim, A., Amis, E.J., Vanlandingham, M.R., Kim, H.-C., Volksen, W., Miller, R.D., Simonyi, E.E., 2004. A buckling-based metrology for measuring the elastic moduli of polymeric thin films. Nat. Mater. 3 (8), 545–550.

Sun, J.-Y., Xia, S., Moon, M.-W., Oh, K.H., Kim, K.-S., 2011. Folding wrinkles of a thin stiff layer on a soft substrate. Proc. R. Soc. A 468 (2140), 932–953.

Supple, W.J., 1967. Coupled branching configurations in the elastic buckling of symmetric structural systems. Int. J. Mech. Sci. 9 (2), 97–112.

Supple, W.J., 1969. Initial post-buckling behaviour of a class of elastic structural systems. Int. J. Non-Linear Mech. 4 (1), 23–36.

Supple, W.J., 1970. Changes of wave-form of plates in the post-buckling range. Int. J. Solids Struct. 6 (9), 1243–1258.

Volynskii, A.L., Bazhenov, S., Lebedeva, O.V., Bakeev, N.F., 2000. Mechanical buckling instability of thin coatings deposited on soft polymer substrates. J. Mater. Sci. 35 (3), 547–554.

Zang, J.F., Zhao, X.H., Cao, Y.P., Hutchinson, J.W., 2012. Localized ridge wrinkling of stiff films on compliant substrates. J. Mech. Phys. Solids 60 (7), 1265–1279.

Zhang, Y., Murphy, K.D., 2005. Secondary buckling and tertiary states of a beam on a non-linear elastic foundation. Int. J. Non-Linear Mech. 40 (6), 795–805.

Zhang, Y., Murphy, K.D., 2013. Jumping instability in the post-buckling of a beam on a partial nonlinear foundation. Acta Mech. Solida Sin. 26 (5), 500–513.